THE JOURNAL OF PHYSICAL CHEMISTRY LETTERS
A JOURNAL OF THE AMERICAN CHEMICAL SOCIETY

pubs.acs.org/JPCL Letter

Tuning Optical Absorption and Emission Using Strongly Coupled Dimers in Programmable DNA Scaffolds

Stephanie M. Hart, Xiao Wang, Jiajia Guo, Mark Bathe,* and Gabriela S. Schlau-Cohen*

Cite This: *J. Phys. Chem. Lett.* 2022, 13, 1863−1871 Read Online

ACCESS | Metrics & More | Article Recommendations | Supporting Information

ABSTRACT: Molecular materials for light harvesting, computing, and fluorescence imaging require nanoscale integration of electronically active subunits. Variation in the optical absorption and emission properties of the subunits has primarily been achieved through modifications to the chemical structure, which is often synthetically challenging. Here, we introduce a facile method for varying optical absorption and emission properties by changing the geometry of a strongly coupled Cy3 dimer on a double-crossover (DX) DNA tile. Leveraging the versatility and programmability of DNA, we tune the length of the complementary strand so that it "pushes" or "pulls" the dimer, inducing dramatic changes in the photophysics including lifetime differences observable at the ensemble and single-molecule level. The separable lifetimes, along with environmental sensitivity also observed in the photophysics, suggest that the Cy3-DX tile constructs could serve as fluorescence probes for multiplexed imaging. More generally, these constructs establish a framework for easily controllable photophysics via geometric changes to coupled chromophores, which could be applied in light-harvesting devices and molecular electronics.

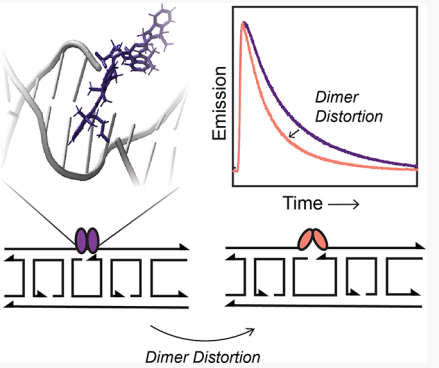

Electronic excited states are used to harness and direct energy from light for a wide range of applications, including fluorescence and sensing assays, data storage, and solar energy conversion.[1−9] For optically addressable molecules, the photophysics have primarily been optimized via synthetic modifications. These modifications, however, frequently require complex chemical syntheses and often result in small changes in the absorption profile and emission properties. Alternatively, the photophysics change dramatically through intermolecular coupling. Variations in coupling have a steep distance dependence that imposes stringent structural requirements[10−14] and so have been much less widely explored.

While meeting these structural requirements has been challenging in many materials,[15−18] the high fidelity of DNA base pairing has allowed for unprecedented control over nanoscale nucleic acid architectures. Canonical double-stranded duplexes are thermodynamically robust, but they have limited applications as a structural building block. In contrast, the DX tile motif, originally inspired by the Holliday junction, is constructed from two long strands and multiple short strands that generate a 2D tile with double the scaffold stiffness as compared to a duplex.[19−21] The DX tile has thus served as a building block for 2D lattices, which have been used in applications such as protein binding, drug delivery, and transition metal binding.[22−26] Furthermore, this type of scaffold engineering has laid the groundwork for three-dimensional nanostructures.[27−33] A large toolkit of modified bases allows for site-specific conjugation of molecules within the DNA structure as well as integration of these constructs into larger-scale devices. Through this capability, molecular chromophores have been scaffolded within DNA in precise and programmable spatial organizations.[34−40] Recent work in this space has focused largely on extending chromophore integration toward DNA origami building blocks including DX tiles and six-helix bundles.[41−43] Despite the potential of this approach, chromophore−DNA constructs have been produced in only a few geometries, limiting the utility of this synthetic platform.

The applications of chromophore−DNA constructs are wide-ranging and include sensing, imaging, and light harvesting. Fluorescent nucleic acids have been used as sensors for metal ions, small molecules, and biomarkers.[13,44−48] Strand displacement reactions, which occur when two strands hybridize displacing a prehybridized strand, have been used to generate optical switches, imaging probes, and multiplexed detection assays.[49−56] Chromophores have also been organized into geometries reminiscent of natural light-harvesting systems for energy capture and transport.[28,39,42,57,58] Chromophores have been precisely positioned by using covalent attachment

Received: November 23, 2021
Accepted: February 14, 2022
Published: February 17, 2022

https://doi.org/10.1021/acs.jpclett.1c03848
J. Phys. Chem. Lett. 2022, 13, 1863−1871

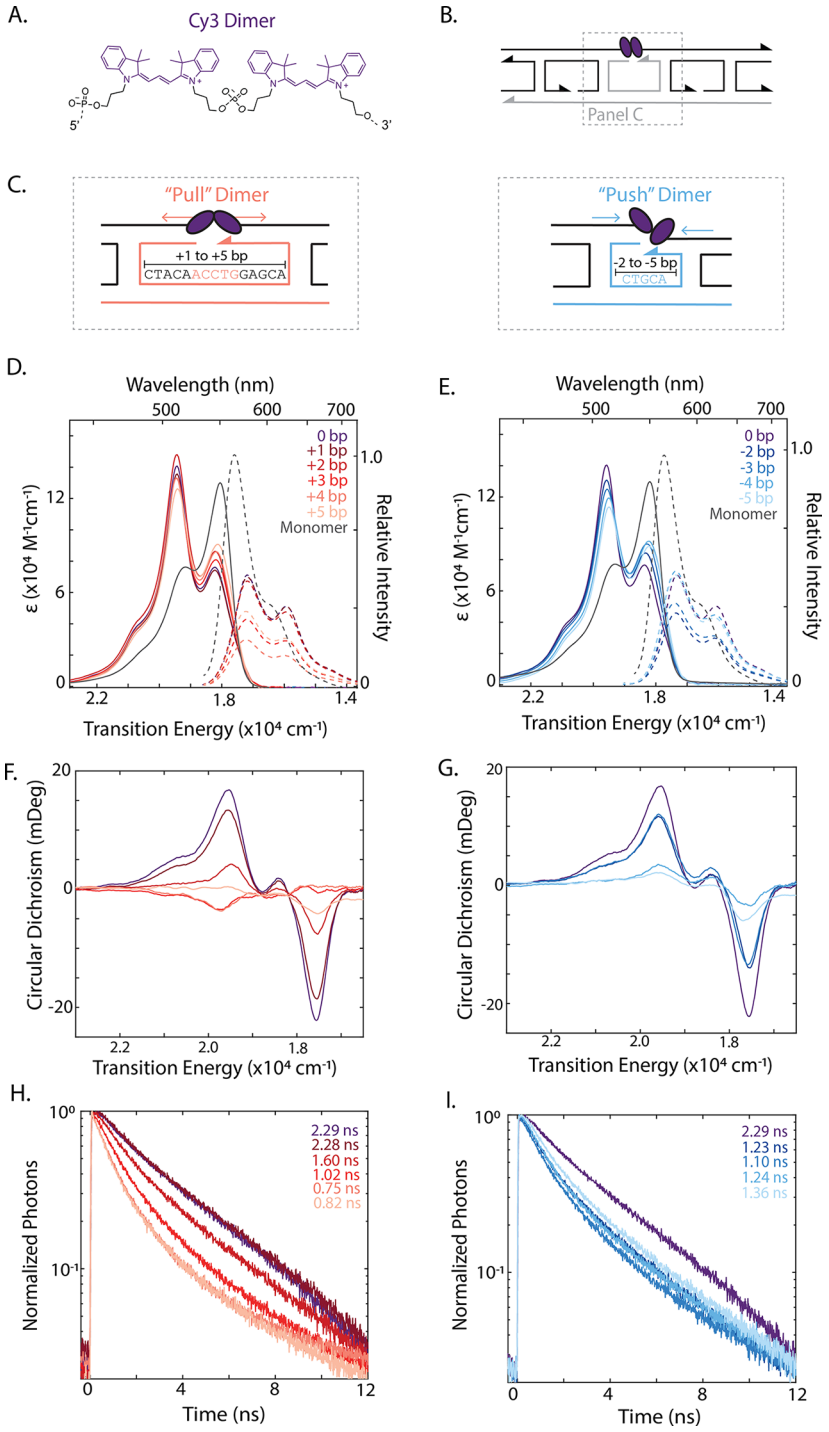

Figure 1. Electronic transitions of Cy3 dimers upon the addition or removal of central crossover strand bases. (A) Chemical structure of the Cy3 dimer. (B) Schematic of the Cy3 dimer that is covalently bridged within a DX tile. The tunable central crossover strand and long strand are shown in gray. (C) Schematic and sequences for Cy3-DX tiles upon the addition (left, "pull"-type) and removal (right, "push"-type) of central crossover and long strand bases. Modified strands are highlighted in light red and light blue for the "pull"-type and "push"-type DX tiles, respectively. Absorption (solid) and emission (dashed) spectra of (D) "pull"-type and (E) "push"-type dimers. Emission spectra are normalized by relative quantum yield for 530 nm excitation. Circular dichroism spectra of (F) "pull"-type and (G) "push"-type dimers. Fluorescence decay traces with 520 nm excitation for dimers formed with the (H) addition, or "push"-type, and (I) removal, or "pull"-type, of central crossover strand bases. Emission was detected at 580 nm.

strategies, including nucleoside modification[29,59,60] and direct incorporation into the DNA backbone,[38,61] which provides control over the photophysics.[42] However, these approaches rely on modifications to the chromophore-containing DNA strands, which limits the tunability and exchangeability of these constructs. Alternatively, molecular aggregates were self-assembled via intercalation[36,62,63] or incorporation within the minor groove.[31,57,58] Despite their more straightforward synthesis, noncovalent approaches lack precise control over the numbers and relative positions of chromophores.

https://doi.org/10.1021/acs.jpclett.1c03848
J. Phys. Chem. Lett. 2022, 13, 1863−1871

Here, we introduce a method to vary the geometry of chromophore dimers scaffolded on a DX tile by varying the length of the strand complementary to the dimer, inspired by previous work describing a DNA nanomechanical device.[64] The tuning of adjacent-DX configurations is achieved by replacing unmodified DNA strands, which do not require the multistep synthesis of the chromophore-containing strand. By addition or removal of bases in the short complementary strand, the distance between adjacent crossovers within the DX tile is increased or decreased, respectively. The changes in distance "push" or "pull" the chromophore dimers, tuning the resultant optical spectrum likely through a decrease in the average intradimer electronic coupling. Measurements using time-resolved fluorescence and transient absorption spectroscopy showed that the variation in electronic coupling led to corresponding differences in the excited-state lifetime. Lifetimes were distinguishable in single-molecule imaging in both time and frequency domain analyses. The dimer excited-state lifetime was also sensitive to local solvent polarity. These results suggest that the Cy3 dimer constructs could serve as fluorescence lifetime imaging (FLIM) probes, for example, to track strand displacement reactions as well as provide a flexible building block for a range of other molecular applications.

Construction and Characterization of Cy3 Dimers. Dimers of indocarbocyanine (Cy3) were incorporated into DNA strands by using phosphoramidite chemistry (Figure 1A).[38] The DX tiles presented here are composed of seven strands: two long 47−57 base strands, which form a structural frame, and five short strands ranging in length from 15 to 25 bases, which "cross over" the long strands in a specific 2D tile geometry (further outlined in Figure S1). DX tiles were assembled by annealing one monomer or dimer containing long strand with one non-chromophore-containing long strand and five non-chromophore containing short crossover strands. We term the short strand complementary to the Cy3 dimer the "central crossover strand". The standard DX tile (Figure 1B) contains a central crossover strand with 20 bases (denoted as "0 bp"), with the corresponding 52 bases in the non-chromophore long strand. We can tune the Cy3 dimer photophysics exclusively with non-chromophore-containing strands by adjusting the length of just two strands: the central crossover strand and the non-chromophore-containing long strand shown in gray in Figure 1B. The DX tiles designed to pull the Cy3 dimers apart (Figure 1C, left) contain a central crossover strand with 21−25 bases ("+1 to +5 bp"), while the long strand contains 53−57 bases. The DX tiles designed to push the Cy3 dimers together (Figure 1C, right) contain a central crossover strand with 15−18 bases ("−5 to −2 bp"), with a long strand containing 47−50 bases. The separation of each folded DX tile construct was confirmed through polyacrylamide gel electrophoresis (PAGE) analyses (Figures S2 and S3).

The optical properties of the Cy3 dimers were initially investigated by comparing their linear absorption spectra. The spectra for all the dimers are shown in Figure 1D,E. The spectra exhibited a redistribution of oscillator strength from the 0−0 to the 0−1 band as well as a hypsochromic shift in the transition energy for the 0 bp Cy3 dimer in comparison to the monomer (dark gray). Both of these features are spectroscopic signatures of a vibronically coupled subradiant "H-type" aggregate,[65,66] which is generated through cofacial stacking of the chromophores. The quantum yields (Table S4) were also lower than the monomer, consistent with the subradiant nature of the H-type dimer. In Figure 1F,G, the circular dichroism (CD) spectra of the 0 bp Cy3 dimers show a bisignate line shape, where the signs of the observed peaks have been assigned to a vibronically coupled H-aggregate.[67,68] The formation of an H-type dimer is consistent with previous findings that Cy3 dimers on the same strand of DNA stack largely cofacially.[42]

The addition or removal of base pairs from the central crossover strand results in a concomitant reduction in the difference in relative intensity between the 0−0 and 0−1 vibronic band (Figure 1D,E; Tables S3 and S4), indicating a diminution of electronic coupling. A decrease in the intensity of the bisignate peaks in the circular dichroism spectra of the Cy3-DX constructs upon addition or subtraction of base pairs further corroborates the assignment to diminution of coupling (Figure 1F,G). The changes in the CD spectra, as well as the previously established pushing and pulling forces applied by the DX tile scaffold,[64] imply that the length of the complementary strand induces geometric changes to the Cy3 dimers. We thereby ascribe the molecular origin of the observed variation in optical properties to be these geometric changes. The disruption of the structure for the dimer chiral response points to a change in stacking contributing to the measured spectroscopic signatures, particularly for the "pull"-type dimer where changes in the spectral profiles are observed for the +3 bp to +5 bp constructs. The observed spectral changes could arise from a combination of a discrete decrease in electronic coupling toward a monomer-like species and/or transition from cofacial stacking to head-to-tail, reducing the magnitude of electronic coupling.[65,66] However, the observed changes in chiral response could also arise from formation of a subpopulation of dimers with opposite handedness from the 0 bp dimer, thus contributing to interfering CD signals. Despite the spectral signatures corresponding to a decrease in electronic coupling, several of the dimers (+3 bp, +4 bp, +5 bp, −2 bp, and −3 bp) showed a decreased quantum yield, which could be a result of aggregation-induced nonradiative decay pathways.[34,69]

DNA Structure Tunes Dimer Photophysics. Structural distortions, such as those induced by the addition and removal of base pairs to the central crossover strand, vary the resultant excited-state dynamics used in many of the applications of DNA−chromophore assemblies. To characterize the overall excited-state temporal evolution, time-correlated single photon counting (TCSPC) was used to measure the emissive lifetime. The Cy3 monomer, a single cyanine chromophore bound within the DX tile, has an average lifetime of 1.5 ns (structure and lifetime data are shown in Figure S9). The lifetime is composed of two components, 0.6 and 2.1 ns. The Cy3 lifetime in DNA has been previously described by multiexponential kinetics due to different modes of binding to the DNA, which impact the photoisomerization quantum yield and thus the nonradiative decay rate.[70,71] Similar multiexponential effects have also been observed in DX tile scaffolded Cy3 monomers.[42] The 0 bp dimer exhibits a biexponential decay with a 0.29 ± 0.02 and a 3.40 ± 0.05 ns component, which gave an average lifetime of 2.3 ns. The two components likely correspond to static and/or dynamic subpopulations within the DNA scaffold with different geometries. The long component is likely from the subradiant emission of the H-aggregate, and the short component is likely from a fast nonradiative decay pathway. Additional dimer geometries or monomer-like subpopulations could also be present. However, additional

https://doi.org/10.1021/acs.jpclett.1c03848
J. Phys. Chem. Lett. 2022, 13, 1863−1871

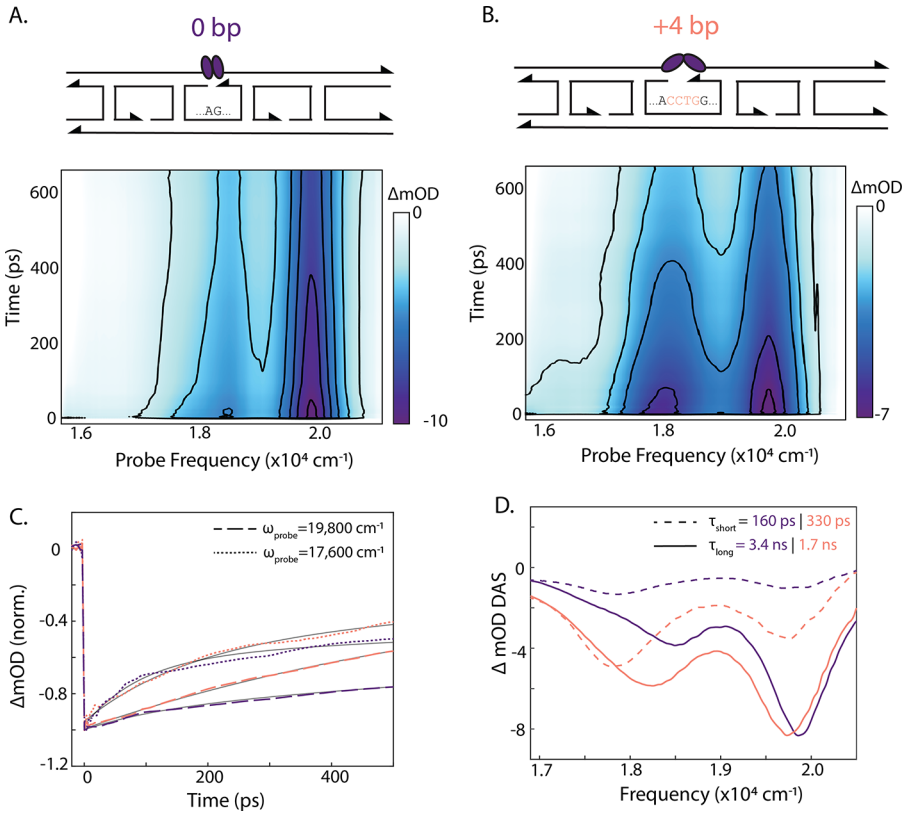

Figure 2. Ultrafast transient absorption spectra identify two subpopulations. (A) Broadband transient absorption spectra of 0 bp dimer and (B) + 4 bp dimer (excitation centered at 540 nm). (C) Transient absorption kinetic traces from (A) and (B) at 19800 and 17600 cm^{-1} for 0 bp (purple) and +4 bp dimer (red). (D) Globally fit decay associated spectra (DAS) of (A) and (B) for 0 bp and +4 bp. The long time scale is shown as solid lines (τ = 4 ns and τ = 1.7 ns for 0 and +4 bp, respectively), and the short time scale is shown as dashed lines (τ = 160 ps and τ = 330 ps for 0 and +4 bp, respectively). The +4 bp DAS is scaled by a factor of 1.7 for ease of visualization.

exponential terms were not required to achieve a good fit, suggesting the additional species, if any, have similar lifetimes. Work on both Cy3 and Cy5 dimers formed on opposite strands of DNA has identified subpopulations of both J- and H-type dimers,[35,69,72] while Cy3 dimers formed on the same strand as in this work appear to have strongly coupled H-type populations and weak H-type or weak J-type populations.[42] Similar heterogeneity in electronic coupling within molecular aggregates has also been observed beyond dimer assemblies.[73−75]

The addition or removal of central crossover strand bases lowered the average lifetime from 2.3 ns to a minimum of 0.8 ns, as shown in Figure 1. The lower values arise from the long-lifetime component shortening from 3.4 to 1.7 ns and the short-lifetime component increasing in amplitude (Table S5). In conjunction with the quantum yield, these results show a suppressed radiative rate for all dimers relative to the monomer, further indicative of H-type aggregation. The 0 bp dimer shows the slowest radiative rate, while addition and removal of bases to the central crossover strand results in an increase in both the radiative and nonradiative rates (Table S5). In agreement with absorption and CD measurements, the increase in radiative rates relative to the 0 bp dimer points toward either a decrease in the magnitude of electronic coupling or an increase in subpopulations of weakly coupled dimers or monomer-like species. The nonradiative rate is likely increased by an enhancement in either isomerization, as has been previously observed in Cy3 dimers,[35] or internal conversion driven by strong nonadiabatic coupling, as has been observed in Cy5 J- and H-aggregates.[34] Collectively, these results highlight the utility of geometric changes in tuning photophysics via both the excitonic radiative decay and the nonradiative decay, which is often determined by the environment.

To gain further insight into the nature of the excited states, ultrafast transient absorption spectra were measured for the 0 bp and +4 bp dimers, which show the longest and shortest lifetimes, respectively (Figure 2A,B). Within the spectral region probed, both dimers showed negative peaks from ground-state bleach/stimulated emission signal at the 0−0 and 0−1 transitions. The decay of the negative peaks was well fit with biexponential kinetics. The long-time component was held constant at the value of the emission lifetime (3.4 ns for 0 bp and 1.7 ns for +4 bp), with the time scale of the short component as a free parameter. The recovered time scales were 160 and 330 ps for 0 bp and +4 bp, respectively. The short components may reflect a subpopulation of weakly coupled dimers or aggregation-induced nonradiative decay, which was observed previously and assigned to a torsional motion.[34,35,69,72] The long components likely arise from H-type dimers, where the slower time scale for the 0 bp dimer indicates stronger electronic coupling, consistent with the conclusions from the steady-state spectra and fluorescence lifetimes.

Global analysis using a two-component parallel decay model was used to extract the decay associated spectra (DAS) for both kinetic components, as shown in Figure 2D. While both the 0−0 and 0−1 peaks are present in all the DAS, the 0−0/

https://doi.org/10.1021/acs.jpclett.1c03848
J. Phys. Chem. Lett. 2022, 13, 1863−1871

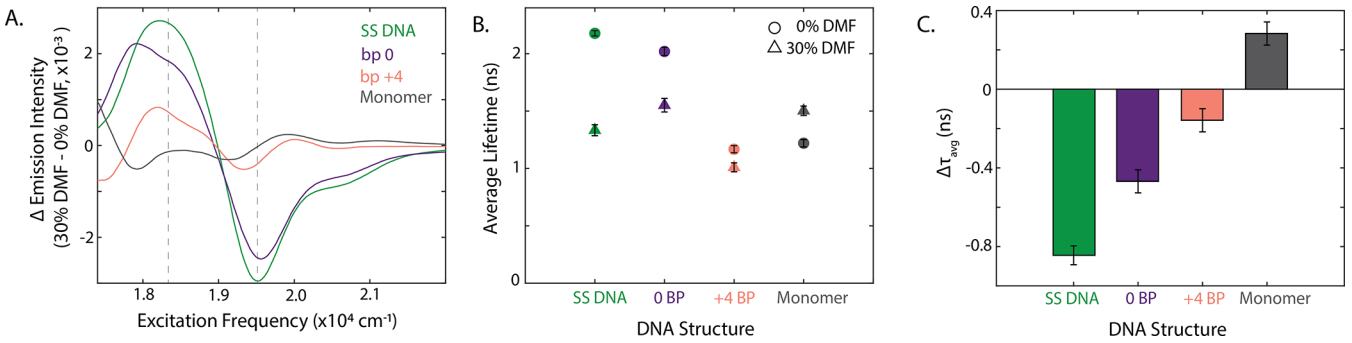

Figure 3. Emission changes with environment polarity. (A) Change in excitation spectrum under addition of 30% DMF (relative to area normalized spectrum in 0% DMF, 624 nm emission). Dashed lines indicate the 0−0 and 0−1 transitions for the 0 bp dimer. (B) Average emission lifetimes upon 545 nm excitation for Cy3 dimers within 0 bp and +4 bp DX tiles and single-stranded DNA and for Cy3 monomers within 0 bp DX tiles in 0% DMF and 30% DMF. Emitted photons were detected at 580 nm. (C) Difference in average lifetime (30% DMF − 0% DMF) for DNA constructs.

0−1 band ratio was larger for the short component DAS than for the long component DAS. The larger ratio is consistent with the assignment of the short component to subpopulations with weaker H-type electronic coupling. The smaller 0−0/0−1 band ratio of the long component DAS is indicative of the strong H-type electronic coupling in this subpopulation. The 0−0/0−1 band ratio for both DAS of the 0 bp dimer is smaller than for the +4 bp dimer, as expected for the stronger H-type electronic coupling in the 0 bp dimer. Collectively, these variations in the excited-state dynamics establish the ability of the complementary strand to induce changes in geometry and provide flexible building blocks for light harvesting, computing, and imaging applications.

Environmental Sensitivity of Dimer Constructs. One method for chemical sensing exploits the environmental sensitivity of fluorescence as a reporter of the local composition.[76−78] Cy3 is likely to exhibit such sensitivity as it is highly susceptible to environmental changes due to its hydrophobic regions and propensity for photoisomerization.[71,79,80] We investigated the environmental sensitivity of the Cy3 dimers by measuring the impact of solvent polarity on their emission. We characterized single-stranded, 0 bp and +4 bp dimers by comparing a buffered solution of 70% water and 30% dimethylformamide (DMF) to a buffered aqueous solution. The fluorescence excitation spectra (Figure S12) report on the relative contributions of the optical transitions to emission. The difference excitation spectra between 0% DMF and 30% DMF are shown for all three samples in Figure 3A. The oscillator strength was redistributed from the 0−1 to the 0−0 band and approaches the monomer spectrum, indicating a larger population of weakly coupled dimers in the less polar environment. Similar changes were also observed in the absorption spectra (Figure S13). The transition dipole moment is localized on a primarily hydrophobic region, which may lead to weaker interdye interaction in the less polar environment.

The average lifetimes for the three samples are shown in Figure 3B. The average lifetime of the single-stranded DNA was the longest at 2.2 ns, and the lifetimes of 0 bp and +4 bp DX tiles shortened to 2.0 and 1.2 ns, respectively. In the 30% DMF solution, all the lifetimes shortened with the largest change for the single-stranded DNA and the smallest for the +4 bp dimer (Figure 3B,C). In contrast, the lifetime of the monomer increased slightly, similar to previous work on the polarity-dependent behavior of cyanine dyes.[81]

The large change for single-stranded DNA likely arises from the lack of structural constraints, which allows for the closest cofacial stacking, and thus the longest lifetime in aqueous solution, as well as the easiest formation of amonomer-like population, which shortens the lifetime in 30% DMF. The small change for the +4 bp dimer is likely due to the longer central crossover strand pulling the dimers apart, resulting in an extended configuration with less cofacial stacking and less freedom to adopt a monomer-like configuration. Consistent with this picture, the +4 bp dimer has a shorter lifetime in 100% aqueous solution, i.e., smaller H-type coupling, and a minimal decrease in lifetime upon addition of 30% DMF, i.e., limited structural rearrangement. Overall, these observations of a polarity-based solvent dependence establish a mechanism to read out the properties of the local environment.

Probes for Fluorescence Lifetime Imaging. Fluorescence lifetime imaging (FLIM) is widely used to map out biological and materials systems based on differences in the lifetime of fluorescent probes or the material itself. This imaging modality requires separation between lifetimes with high sensitivity and fidelity.[82,83] While this has typically been achieved via synthetic structural modification to chromophore monomers, the large (∼65%) variation in lifetime across the series of Cy3 dimers suggests that tuning dimer geometries, as done here using DNA, may provide an alternate set of FLIM probes for multiplexed imaging. To test the distinguishability of these constructs in FLIM, we performed confocal single-molecule spectroscopy on the 0 bp Cy3 dimer, +4 bp Cy3 dimer, and a 50%/50% mixture of the two dimer constructs. For each sample, the emission of individual Cy3 dimers was recorded, and the emission decay curves were fit to a monoexponential function. The extracted time scales were used to construct lifetime histograms as shown in Figure 4A,C,E. The mean lifetimes were 3.35 and 1.65 ns for the 0 bp and +4 bp dimers, respectively, consistent with the long-lifetime component from the ensemble measurements. The short-lifetime component observed in the ensemble is absent from the single-molecule data due to the longer instrument response function of the high-sensitivity detector.

The standard deviations of the distributions for both the 0 bp and +4 bp dimers were ∼0.5 ns, which is much less than the separation between the mean lifetime of the two samples (3.35 and 1.65 ns, respectively). These results indicate that the 0 bp and +4 bp dimers could be easily distinguished in FLIM imaging. As further confirmation of their distinguishability, the

https://doi.org/10.1021/acs.jpclett.1c03848
J. Phys. Chem. Lett. 2022, 13, 1863−1871

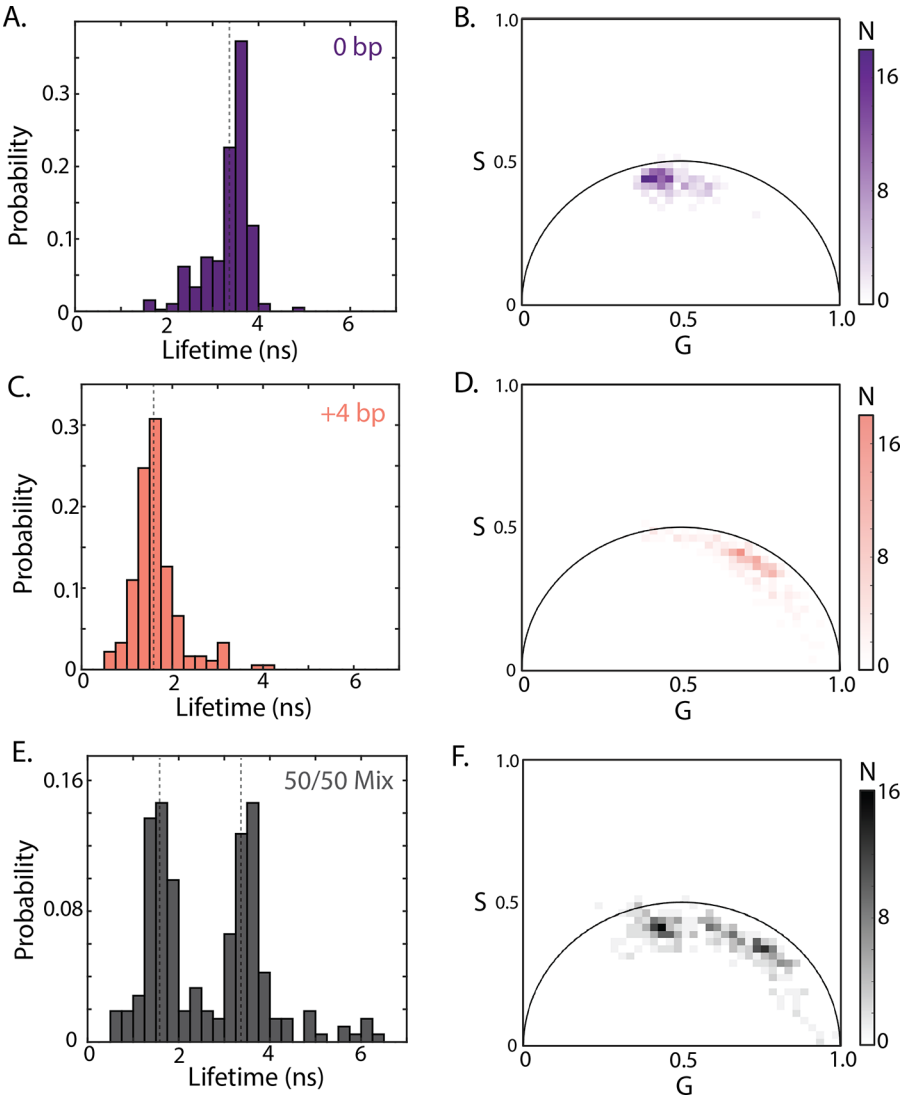

Figure 4. Single-molecule imaging of Cy3-DNA constructs. (A) Distribution of single-molecule emission lifetimes for immobilized samples of 0 bp dimers, (C) +4 bp dimers, and (E) a 50% mixture of 0 bp and +4 bp dimers (550 nm excitation, 590 nm emission). Dashed lines indicate the mean of the 0 bp and +4 bp distributions. (B) Phasor plots calculated according to ref 84 for 0 bp dimers, (D) +4 bp dimers, and (F) a 50% mixture of 0 bp and +4 bp dimers.

data from the 50%/50% mixture were also analyzed. The histogram of the mixture shows a clear bimodal structure (Figure 4E), confirming the two probes could be resolved in FLIM even with the low signal levels intrinsic to single-molecule imaging. The unimodal nature of the single-molecule distributions suggests largely homogeneous populations, although multiple species, such as dimer-like and monomer-like populations, with similar lifetimes could be present.

FLIM experiments are typically performed in the frequency domain for high-throughput data collection. To verify distinguishability of the dimers in the frequency domain, we performed a phasor analysis on the time-domain data, which is a Fourier transform of the decay curves. The Fourier-transformed data are plotted as a function of the real component, G, and the imaginary component, S, of the frequency domain response as shown in Figure 4B,D,F.[82,85,86] The lifetime is proportional to the ratio of S to G in the frequency domain signal, and thus each distribution of single molecules corresponds to distinct populations in the phase space maps (Figure 4B,D). The center of the 0 bp distribution appears at (G = 0.45, S = 0.43), while the center of the +4 bp distribution occurs at (G = 0.70, S = 0.37). Although the +4 bp distribution is broader, the 0 bp and +4 bp dimers are confined above and below G = 0.5, respectively. Similar to the time domain results, the distribution of the 50%/50% mixture in phase space has two clear populations separated by a region with a near-zero population (Figure 4E), establishing that these two constructs are also distinguishable in the frequency domain.

The distinguishability of the Cy3 dimers establishes their utility as FLIM probes. Furthermore, the changes in emission spectra and lifetime with solvent polarity allow the dimers to report on their local environment within a FLIM/multiplexed measurement. Indeed, FLIM probes are often used to detect changes in chemical environment, including polarity as well as pH, analyte concentration, and viscosity, which were previously established to also change the Cy3 emission.[35,71,83] The central crossover strand dependence of the lifetime also allows for facile tracking of strand displacement reactions. Precise knowledge of the kinetics of these reactions is often

https://doi.org/10.1021/acs.jpclett.1c03848
J. Phys. Chem. Lett. 2022, 13, 1863−1871

exploited to deploy DNA in analyte sensing.[87,88] Beyond strand displacement reactions, the dependence of the photophysics on the complementary central crossover strand has the potential to enable studies of DNA hybridization and other properties of nucleic acids.[89] Finally, the DNA scaffold means that the construct is biocompatible and easily functionalized for specific conjugation to desired targets.

Here, we report a method to introduce geometric changes to DNA-scaffolded Cy3 dimers via the central crossover strand, thereby tuning the corresponding photophysical properties such as the optical spectrum and emission lifetime. Based on the length of the strand, the DNA scaffold pushed or pulled the dimers, changing the geometry and as a result changing the transition energies, fluorescence lifetime, and solvent dependence of the excited states. In particular, the solvent-dependent lifetimes and distinguishability between dimers of different geometries at the single-molecule level suggest these constructs could serve as FLIM probes. Overall, the photophysical variations in interchromophore interaction drive changes in the excited-state dynamics, which may be used in fluorescence assays, light harvesting devices, and molecular electronics.

■ ASSOCIATED CONTENT

Supporting Information

The Supporting Information is available free of charge at https://pubs.acs.org/doi/10.1021/acs.jpclett.1c03848.

Information regarding sample preparation methods, DNA construct design and sample purification, and spectroscopic characterization and analysis methods; tables and figures including additional monomer and dimer spectroscopic characterization and analysis including quantum yield, vibronic band ratio, excitation spectra, circular dichroism, and calculated radiative and nonradiative decay rates; solvent-dependent absorption, emission, and excitation spectra and TCSPC traces as well as exemplary single-molecule spectroscopy and transient absorption global fitting results (PDF)

■ AUTHOR INFORMATION

Corresponding Authors

Mark Bathe − *Department of Biological Engineering, Massachusetts Institute of Technology, Cambridge, Massachusetts 02139, United States;* orcid.org/0000-0002-6199-6855; Email: mbathe@mit.edu

Gabriela S. Schlau-Cohen − *Department of Chemistry, Massachusetts Institute of Technology, Cambridge, Massachusetts 02139, United States;* orcid.org/0000-0001-7746-2981; Email: gssc@mit.edu

Authors

Stephanie M. Hart − *Department of Chemistry, Massachusetts Institute of Technology, Cambridge, Massachusetts 02139, United States*

Xiao Wang − *Department of Biological Engineering, Massachusetts Institute of Technology, Cambridge, Massachusetts 02139, United States*

Jiajia Guo − *Department of Chemistry, Massachusetts Institute of Technology, Cambridge, Massachusetts 02139, United States;* Present Address: Center for Bionic Sensing and Intelligence, Institute of Biomedical and Health Engineering, Shenzhen Institute of Advanced Technology, Chinese Academy of Sciences Shenzhen 518055, China; orcid.org/0000-0002-6118-8241

Complete contact information is available at: https://pubs.acs.org/10.1021/acs.jpclett.1c03848

Author Contributions

S.M.H. and X.W. contributed equally to this work.

Notes

The authors declare the following competing financial interest(s): The Massachusetts Institute of Technology has filed a patent on tunable DNA-dye single-molecule imaging probes on behalf of the inventors Gabriela S. Schlau-Cohen, Mark Bathe, Stephanie M. Hart, Xiao Wang, and Jiajia Guo.

■ ACKNOWLEDGMENTS

This work was primarily supported by the U.S. Department of Energy, Office of Science, Office of Basic Energy Sciences, Division of Materials Sciences and Engineering, under Award # DE-SC0019998 to M.B. and G.S.S.-C. The single-molecule measurements were supported by the National Science Foundation (NSF) RAISE TAQS under Award # 1839155 to M.B. and G.S.S.-C. Funding from the ARO ICB Subaward KK1954 to X.W. and M.B. is gratefully acknowledged. S.M.H. acknowledges support from the NSF Graduate Research Fellowship Program. The authors thank Dr. James Banal for helpful discussions in the construction of this manuscript.

■ REFERENCES

(1) Lichtman, J. W.; Conchello, J.-A. Fluorescence Microscopy. *Nat. Methods* **2005**, *2*, 910−919.

(2) Wang, Q.; Wang, W.; Lei, J.; Xu, N.; Gao, F.; Ju, H. Fluorescence Quenching of Carbon Nitride Nanosheet Through its Interaction with DNA for Versatile Fluorescence Sensing. *Anal. Chem.* **2013**, *85*, 12182−12188.

(3) Yuan, L.; Lin, W.; Zheng, K.; He, L.; Huang, W. Far-red to Near Infrared Analyte-responsive Fluorescent Probes Based on Organic Fluorophore Platforms for Fluorescence Imaging. *Chem. Soc. Rev.* **2013**, *42*, 622−661.

(4) Banal, J. L.; Shepherd, T. R.; Berleant, J.; Huang, H.; Reyes, M.; Ackerman, C. M.; Blainey, P. C.; Bathe, M. Random Access DNA Memory Using Boolean Search in an Archival File Storage System. *Nat. Mater.* **2021**, *20*, 1272−1280.

(5) Mottaghi, M. D.; Dwyer, C. Thousand-fold Increase in Optical Storage Density by Polychromatic Address Multiplexing on Self-assembled DNA Nanostructures. *Adv. Mater.* **2013**, *25*, 3593−3598.

(6) Blankenship, R. E. *Molecular Mechanisms of Photosynthesis*; John Wiley & Sons: New York, 2014.

(7) Cheng, Y.-C.; Fleming, G. R. Dynamics of Light Harvesting in Photosynthesis. *Annu. Rev. Phys. Chem.* **2009**, *60*, 241−262.

(8) Romero, E.; Novoderezhkin, V.; van Grondelle, R. Quantum Design of Photosynthesis for Bio-inspired Solar-energy Conversion. *Nature* **2017**, *543*, 355−365.

(9) Brédas, J.-L.; Sargent, E.; Scholes, G. Photovoltaic Concepts Inspired by Coherence Effects in Photosynthetic Systems. *Nat. Mater.* **2017**, *16*, 35−44.

(10) Schröter, M.; Ivanov, S. D.; Schulze, J.; Polyutov, S. P.; Yan, Y.; Pullerits, T.; Kühn, O. Exciton-vibrational Coupling in the Dynamics and Spectroscopy of Frenkel Excitons in Molecular Aggregates. *Phys. Rep.* **2015**, *567*, 1−78.

(11) Fleming, G. R.; Schlau-Cohen, G. S.; Amarnath, K.; Zaks, J. Design Principles of Photosynthetic Light-harvesting. *Faraday Discuss.* **2012**, *155*, 27−41.

(12) Delor, M.; Dai, J.; Roberts, T. D.; Rogers, J. R.; Hamed, S. M.; Neaton, J. B.; Geissler, P. L.; Francis, M. B.; Ginsberg, N. S. Exploiting Chromophore-protein Interactions Through Linker Engineering to

Tune Photoinduced Dynamics in a Biomimetic Light-harvesting Platform. *J. Am. Chem. Soc.* **2018**, *140*, 6278−6287.
(13) Yang, F.; Li, Q.; Wang, L.; Zhang, G.-J.; Fan, C. Framework-nucleic-acid-enabled Biosensor Development. *ACS Sens* **2018**, *3*, 903−919.
(14) Teles, F.; Fonseca, L. Trends in DNA Biosensors. *Talanta* **2008**, *77*, 606−623.
(15) Scholes, G. D.; Rumbles, G. Excitons in Nanoscale Systems. *Nat. Mater.* **2010**, 12−25.
(16) Fassioli, F.; Dinshaw, R.; Arpin, P. C.; Scholes, G. D. Photosynthetic Light Harvesting: Excitons and Coherence. *J. R. Soc. Interface* **2014**, *11*, 20130901.
(17) Scholes, G. D.; Fleming, G. R.; Chen, L. X.; Aspuru-Guzik, A.; Buchleitner, A.; Coker, D. F.; Engel, G. S.; van Grondelle, R.; Ishizaki, A.; Jonas, D. M.; et al. Using Coherence to Enhance Function in Chemical and Biophysical Systems. *Nature* **2017**, *543*, 647−656.
(18) Castellanos, M. A.; Dodin, A.; Willard, A. P. On the Design of Molecular Excitonic Circuits for Quantum Computing: The Universal Quantum Gates. *Phys. Chem. Chem. Phys.* **2020**, *22*, 3048−3057.
(19) Fu, T. J.; Seeman, N. C. DNA Double-crossover Molecules. *Biochemistry* **1993**, *32*, 3211−3220.
(20) Sa-Ardyen, P.; Vologodskii, A. V.; Seeman, N. C. The Flexibility of DNA Double Crossover Molecules. *Biophys. J.* **2003**, *84*, 3829−3837.
(21) Li, X.; Yang, X.; Qi, J.; Seeman, N. C. Antiparallel DNA Double Crossover Molecules as Components for Nanoconstruction. *J. Am. Chem. Soc.* **1996**, *118*, 6131−6140.
(22) Winfree, E.; Liu, F.; Wenzler, L. A.; Seeman, N. C. Design and Self-assembly of Two-dimensional DNA Crystals. *Nature* **1998**, *394*, 539−544.
(23) Jun, H.; Zhang, F.; Shepherd, T.; Ratanalert, S.; Qi, X.; Yan, H.; Bathe, M. Autonomously Designed Free-form 2D DNA Origami. *Sci. Adv.* **2019**, *5*, No. eaav0655.
(24) Cohen, J. D.; Sadowski, J. P.; Dervan, P. B. Programming Multiple Protein Patterns on a Single DNA Nanostructure. *J. Am. Chem. Soc.* **2008**, *130*, 402−403.
(25) Chao, J.; Liu, H.; Su, S.; Wang, L.; Huang, W.; Fan, C. Structural DNA Nanotechnology for Intelligent Drug Delivery. *Small* **2014**, *10*, 4626−4635.
(26) Rousina-Webb, A.; Lachance-Brais, C.; Rizzuto, F. J.; Askari, M. S.; Sleiman, H. F. Transition-Metal-Functionalized DNA Double-Crossover Tiles: Enhanced Stability and Chirality Transfer to Metal Centers. *Angew. Chem., Int. Ed.* **2020**, *59*, 4091−4098.
(27) Garo, F.; Häner, R. A DNA-based Light-harvesting Antenna. *Angew. Chem.* **2012**, *51*, 916−919.
(28) Dutta, P. K.; Varghese, R.; Nangreave, J.; Lin, S.; Yan, H.; Liu, Y. DNA-Directed Artificial Light-harvesting Antenna. *J. Am. Chem. Soc.* **2011**, *133*, 11985−11993.
(29) Ensslen, P.; Wagenknecht, H.-A. One-dimensional Multi-chromophor Arrays Based on DNA: From Self-assembly to Light-harvesting. *Acc. Chem. Res.* **2015**, *48*, 2724−2733.
(30) Melinger, J. S.; Sha, R.; Mao, C.; Seeman, N. C.; Ancona, M. G. Fluorescence and Energy Transfer in Dye-labeled DNA Crystals. *J. Phys. Chem. B* **2016**, *120*, 12287−12292.
(31) Boulais, E.; Sawaya, N. P. D.; Veneziano, R.; Andreoni, A.; Banal, J. L.; Kondo, T.; Mandal, S.; Lin, S.; Schlau-Cohen, G. S.; Woodbury, N. W.; et al. Programmed Coherent Coupling in a Synthetic DNA-based Excitonic Circuit. *Nat. Mater.* **2018**, *17*, 159−166.
(32) Wamhoff, E.-C.; Banal, J. L.; Bricker, W. P.; Shepherd, T. R.; Parsons, M. F.; Veneziano, R.; Stone, M. B.; Jun, H.; Wang, X.; Bathe, M. Programming Structured DNA Assemblies to Probe Biophysical Processes. *Annu. Rev. Biophys.* **2019**, *48*, 395−419.
(33) Seeman, N. C. An Overview of Structural DNA Nanotechnology. *Mol. Biotechnol.* **2007**, *37*, 246.
(34) Huff, J. S.; Davis, P. H.; Christy, A.; Kellis, D. L.; Kandadai, N.; Toa, Z. S.; Scholes, G. D.; Yurke, B.; Knowlton, W. B.; Pensack, R. D. DNA-templated Aggregates of Strongly Coupled Cyanine Dyes: Nonradiative Decay Governs Exciton Lifetimes. *J. Phys. Chem. Lett.* **2019**, *10*, 2386−2392.
(35) Cunningham, P. D.; Kim, Y. C.; Diaz, S. A.; Buckhout-White, S.; Mathur, D.; Medintz, I. L.; Melinger, J. S. Optical Properties of Vibronically Coupled Cy3 Dimers on DNA Scaffolds. *J. Phys. Chem. B* **2018**, *122*, 5020−5029.
(36) Cunningham, P. D.; Bricker, W. P.; Díaz, S. A.; Medintz, I. L.; Bathe, M.; Melinger, J. S. Optical Determination of the Electronic Coupling and Intercalation Geometry of Thiazole Orange Homodimer in DNA. *J. Chem. Phys.* **2017**, *147*, 055101.
(37) Cannon, B. L.; Kellis, D. L.; Patten, L. K.; Davis, P. H.; Lee, J.; Graugnard, E.; Yurke, B.; Knowlton, W. B. Coherent Exciton Delocalization in a Two-state DNA-templated Dye Aggregate System. *J. Phys. Chem. A* **2017**, *121*, 6905−6916.
(38) Markova, L. I.; Malinovskii, V. L.; Patsenker, L. D.; Häner, R. J-vs. H-type Assembly: Pentamethine Cyanine (Cy5) as a Near-IR Chiroptical Reporter. *Chem. Commun.* **2013**, *49*, 5298−5300.
(39) Sohail, S. H.; Otto, J. P.; Cunningham, P. D.; Kim, Y. C.; Wood, R. E.; Allodi, M. A.; Higgins, J. S.; Melinger, J. S.; Engel, G. S. DNA Scaffold Supports Long-lived Vibronic Coherence in an Indodicarbocyanine (Cy5) Dimer. *Chem. Sci.* **2020**, *11*, 8546−8557.
(40) Kringle, L.; Sawaya, N. P. D.; Widom, J.; Adams, C.; Raymer, M. G.; Aspuru-Guzik, A.; Marcus, A. H. Temperature-dependent Conformations of Exciton-Coupled Cy3 Dimers in Double-stranded DNA. *J. Chem. Phys.* **2018**, *148*, 085101.
(41) Mathur, D.; Kim, Y. C.; Díaz, S. A.; Cunningham, P. D.; Rolczynski, B. S.; Ancona, M. G.; Medintz, I. L.; Melinger, J. S. Can a DNA Origami Structure Constrain the Position and Orientation of an Attached Dye Molecule? *J. Phys. Chem. C* **2021**, *125*, 1509.
(42) Hart, S. M.; Chen, W. J.; Banal, J. L.; Bricker, W. P.; Dodin, A.; Markova, L.; Vyborna, Y.; Willard, A. P.; Haner, R.; Bathe, M.; Schlau-Cohen, G. S. Engineering Couplings for Exciton Transport using Synthetic DNA Scaffolds. *Chem.* **2021**, *7*, 752−773.
(43) Mazuski, R. J.; Díaz, S. A.; Wood, R. E.; Lloyd, L. T.; Klein, W. P.; Mathur, D.; Melinger, J. S.; Engel, G. S.; Medintz, I. L. Ultrafast Excitation Transfer in Cy5 DNA Photonic Wires Displays Dye Conjugation and Excitation Energy Dependency. *J. Phys. Chem. Lett.* **2020**, *11*, 4163−4172.
(44) Yang, D.; Liu, X.; Zhou, Y.; Luo, L.; Zhang, J.; Huang, A.; Mao, Q.; Chen, X.; Tang, L. Aptamer-based Biosensors for Detection of Lead (II) Ion: A Review. *Anal. Methods* **2017**, *9*, 1976−1990.
(45) Tan, S. S.; Kim, S. J.; Kool, E. T. Differentiating Between Fluorescence-quenching Metal Ions with Polyfluorophore Sensors Built on a DNA Backbone. *J. Am. Chem. Soc.* **2011**, *133*, 2664−2671.
(46) Walter, H.-K.; Bauer, J.; Steinmeyer, J.; Kuzuya, A.; Niemeyer, C. M.; Wagenknecht, H.-A. DNA Origami Traffic Lights" With a Split Aptamer Sensor for a Bicolor Fluorescence Readout. *Nano Lett.* **2017**, *17*, 2467−2472.
(47) Dai, N.; Teo, Y. N.; Kool, E. T. DNA-polyfluorophore Excimers as Sensitive Reporters for Esterases and Lipases. *Chem. Commun.* **2010**, *46*, 1221−1223.
(48) Chen, H.; Wu, S.; Dong, F.; Cheng, W.; Li, Q.; Ding, S.; Luo, R. A Novel Chemiluminescence Immunoassay for Highly Sensitive and Specific Detection of Protein Using Rolling Circle Amplification and the Multiplex Binding System. *Sens. Actuators B Chem.* **2015**, *221*, 328−333.
(49) Cannon, B. L.; Kellis, D. L.; Davis, P. H.; Lee, J.; Kuang, W.; Hughes, W. L.; Graugnard, E.; Yurke, B.; Knowlton, W. B. Excitonic AND Logic Gates on DNA Brick Nanobreadboards. *ACS Photonics* **2015**, *2*, 398−404.
(50) Kellis, D. L.; Rehn, S. M.; Cannon, B. L.; Davis, P. H.; Graugnard, E.; Lee, J.; Yurke, B.; Knowlton, W. B. DNA-mediated Excitonic Upconversion FRET Switching. *New J. Phys.* **2015**, *17*, 115007.
(51) Uno, S.-n.; Dohno, C.; Bittermann, H.; Malinovskii, V. L.; Häner, R.; Nakatani, K. A Light-driven Supramolecular Optical Switch. *Angew. Chem.* **2009**, *121*, 7498−7501.
(52) Abdollahi, E.; Taucher-Scholz, G.; Jakob, B. Application of Fluorescence Lifetime Imaging Microscopy of DNA Binding Dyes to

https://doi.org/10.1021/acs.jpclett.1c03848
J. Phys. Chem. Lett. 2022, 13, 1863−1871

Assess Radiation-induced Chromatin Compaction Changes. *Int. J. Mol. Sci.* **2018**, *19*, 2399.
(53) Tseng, T.-Y.; Chien, C.-H.; Chu, J.-F.; Huang, W.-C.; Lin, M.-Y.; Chang, C.-C.; Chang, T.-C. Fluorescent Probe for Visualizing Guanine-quadruplex DNA by Fluorescence Lifetime Imaging Microscopy. *J. Biomed. Opt.* **2013**, *18*, 101309.
(54) Qiu, X.; Guo, J.; Xu, J.; Hildebrandt, N. Three-dimensional FRET Multiplexing for DNA Quantification with Attomolar Detection Limits. *J. Phys. Chem. Lett.* **2018**, *9*, 4379−4384.
(55) Qiu, X.; Guo, J.; Jin, Z.; Petreto, A.; Medintz, I. L.; Hildebrandt, N. Multiplexed Nucleic Acid Hybridization Assays Using Single-FRET-Pair Distance-tuning. *Small* **2017**, *13*, 1700332.
(56) Guo, S.-M.; Veneziano, R.; Gordonov, S.; Li, L.; Danielson, E.; de Arce, K. P.; Park, D.; Kulesa, A. B.; Wamhoff, E.-C.; Blainey, P. C.; et al. Multiplexed and High-throughput Neuronal Fluorescence Imaging with Diffusible Probes. *Nat. Commun.* **2019**, *10*, 1−14.
(57) Banal, J. L.; Kondo, T.; Veneziano, R.; Bathe, M.; Schlau-Cohen, G. S. Photophysics of J-aggregate-mediated Energy Transfer on DNA. *J. Phys. Chem. Lett.* **2017**, *8*, 5827.
(58) Zhou, X.; Mandal, S.; Jiang, S.; Lin, S.; Yang, J.; Liu, Y.; Whitten, D. G.; Woodbury, N. W.; Yan, H. Efficient Long-range, Directional Energy Transfer Through DNA-templated Dye Aggregates. *J. Am. Chem. Soc.* **2019**, *141*, 8473−8481.
(59) Hwang, G. T.; Seo, Y. J.; Kim, B. H. Pyrene-labeled Deoxyuridine and Deoxyadenosine: Fluorescent Discriminating Phenomena in their Oligonucleotides. *Tetrahedron Lett.* **2005**, *46*, 1475−1477.
(60) Seo, Y. J.; Hwang, G. T.; Kim, B. H. Quencher-free Molecular Beacon Systems with Two Pyrene Units in the Stem Region. *Tetrahedron Lett.* **2006**, *47*, 4037−4039.
(61) Vybornyi, M.; Nussbaumer, A. L.; Langenegger, S. M.; Haner, R. Assembling Multiporphyrin Stacks Inside the DNA Double Helix. *Bioconjugate Chem.* **2014**, *25*, 1785−1793.
(62) Günther, K.; Mertig, M.; Seidel, R. Mechanical and Structural Properties of YOYO-1 complexed DNA. *Nucleic Acids Res.* **2010**, *38*, 6526−6532.
(63) Ruedas-Rama, M. J.; Alvarez-Pez, J. M.; Paredes, J. M.; Talavera, E. M.; Orte, A. Binding of BOBO-3 Intercalative Dye to DNA Homo-oligonucleotides with Different Base Compositions. *J. Phys. Chem. B* **2010**, *114*, 6713−6721.
(64) Mao, C.; Sun, W.; Shen, Z.; Seeman, N. C. A Nanomechanical Device Based on the B-Z Transition of DNA. *Nature* **1999**, *397*, 144−146.
(65) Spano, F. C. The Spectral Signatures of Frenkel Polarons in H- and J-aggregates. *Acc. Chem. Res.* **2010**, *43*, 429−439.
(66) Hestand, N. J.; Spano, F. C. Expanded Theory of H-and J-molecular Aggregates: The Effects of Vibronic Coupling and Intermolecular Charge Transfer. *Chem. Rev.* **2018**, *118*, 7069−7163.
(67) Kistler, K.; Pochas, C.; Yamagata, H.; Matsika, S.; Spano, F. Absorption, Circular Dichroism, and Photoluminescence in Perylene Diimide Bichromophores: Polarization-dependent H-and J-aggregate Behavior. *J. Phys. Chem. B* **2012**, *116*, 77−86.
(68) Berova, N.; Nakanishi, K.; Woody, R. W. *Circular Dichroism: Principles and Applications*; John Wiley & Sons: New York, 2000.
(69) Huff, J. S.; Turner, D. B.; Mass, O. A.; Patten, L. K.; Wilson, C. K.; Roy, S. K.; Barclay, M. S.; Yurke, B.; Knowlton, W. B.; Davis, P. H.; et al. Excited-state Lifetimes of DNA-templated Cyanine Dimer, Trimer, and Tetramer Aggregates: The Role of Exciton Delocalization, Dye Separation, and DNA Heterogeneity. *J. Phys. Chem. B* **2021**, *125*, 10240−10259.
(70) Stennett, E. M.; Ma, N.; Van Der Vaart, A.; Levitus, M. Photophysical and Dynamical Properties of Doubly Linked Cy3-DNA Constructs. *J. Phys. Chem. B* **2014**, *118*, 152−163.
(71) Sanborn, M. E.; Connolly, B. K.; Gurunathan, K.; Levitus, M. Fluorescence Properties and Photophysics of the Sulfoindocyanine Cy3 Linked Covalently to DNA. *J. Phys. Chem. B* **2007**, *111*, 11064−11074.
(72) Cunningham, P. D.; Díaz, S. A.; Yurke, B.; Medintz, I. L.; Melinger, J. S. Delocalized Two-exciton States in DNA Scaffolded Cyanine Dimers. *J. Phys. Chem. B* **2020**, *124*, 8042−8049.
(73) Sosa, M. L.; Wong, C. Y. Revealing the Evolving Mixture of Molecular Aggregates During Organic Film Formation Using Simulations of in situ Absorbance. *J. Chem. Phys.* **2020**, *153*, 214902.
(74) Spano, F. C. Absorption and Emission in Oligo-phenylene Vinylene Nanoaggregates: The Role of Disorder and Structural Defects. *J. Chem. Phys.* **2002**, *116*, 5877−5891.
(75) Spano, F. C. Absorption in Regio-regular Poly (3-hexyl) Thiophene Thin Films: Fermi Resonances, Interband Coupling and Disorder. *Chem. Phys.* **2006**, *325*, 22−35.
(76) Wagner, B. D. The Use of Coumarins as Environmentally-sensitive Fluorescent Probes of Heterogeneous Inclusion Systems. *Molecules* **2009**, *14*, 210−237.
(77) Er, J. C.; Tang, M. K.; Chia, C. G.; Liew, H.; Vendrell, M.; Chang, Y.-T. MegaStokes BODIPY-triazoles as Environmentally Sensitive Turn-on Fluorescent Dyes. *Chem. Sci.* **2013**, *4*, 2168−2176.
(78) Shvadchak, V. V.; Kucherak, O.; Afitska, K.; Dziuba, D.; Yushchenko, D. A. Environmentally Sensitive Probes for Monitoring Protein-membrane Interactions at Nanomolar Concentrations. *Biochim. Biophys. Acta - Biomembranes* **2017**, *1859*, 852−859.
(79) Zanetti-Domingues, L. C.; Tynan, C. J.; Rolfe, D. J.; Clarke, D. T.; Martin-Fernandez, M. Hydrophobic Fluorescent Probes Introduce Artifacts into Single Molecule Tracking Experiments Due to Non-specific Binding. *PloS One* **2013**, *8*, No. e74200.
(80) Pace, N. A.; Hennelly, S. P.; Goodwin, P. M. Immobilization of Cyanines in DNA Produces Systematic Increases in Fluorescence Intensity. *J. Phys. Chem. Lett.* **2021**, *12*, 8963−8971.
(81) Lee, H.; Berezin, M. Y.; Henary, M.; Strekowski, L.; Achilefu, S. Fluorescence Lifetime Properties of Near-infrared Cyanine Dyes in Relation to Their Structures. *J. Photochem. Photobio. A* **2008**, *200*, 438−444.
(82) Lakner, P. H.; Monaghan, M. G.; Möller, Y.; Olayioye, M. A.; Schenke-Layland, K. Applying Phasor Approach Analysis of Multi-photon FLIM Measurements to Probe the Metabolic Activity of Three-dimensional in vitro Cell Culture Models. *Sci. Rep.* **2017**, *7*, 1−11.
(83) Gatzogiannis, E.; Chen, Z.; Wei, L.; Wombacher, R.; Kao, Y.-T.; Yefremov, G.; Cornish, V. W.; Min, W. Mapping Protein-specific Micro-environments in Live Cells by Fluorescence Lifetime Imaging of a Hybrid Genetic-chemical Molecular Rotor Tag. *Chem. Commun.* **2012**, *48*, 8694−8696.
(84) Štefl, M.; James, N. G.; Ross, J. A.; Jameson, D. M. Applications of Phasors to in vitro Time-resolved Fluorescence Measurements. *Anal. Biochem.* **2011**, *410*, 62−69.
(85) Martelo, L.; Fedorov, A.; Berberan-Santos, M. N. Fluorescence Phasor Plots Using Time Domain Data: Effect of the Instrument Response Function. *J. Phys. Chem. B* **2015**, *119*, 10267−10274.
(86) Szmacinski, H.; Toshchakov, V.; Lakowicz, J. R. Application of Phasor Plot and Autofluorescence Correction for Study of Heterogeneous Cell Population. *J. Biomed. Opt.* **2014**, *19*, 046017.
(87) Qian, L.; Winfree, E. Scaling Up Digital Circuit Computation With DNA Strand Displacement Cascades. *Science* **2011**, *332*, 1196−1201.
(88) Zhu, J.; Boskovic, F.; Nguyen, B.-N. T.; Nitschke, J. R.; Keyser, U. F. Kinetics of Toehold-mediated DNA Strand Displacement Depend on Fe(II)4L4 Tetrahedron Concentration. *Nano Lett.* **2021**, *21*, 1368−1374.
(89) Israels, B.; Albrecht, C. S.; Dang, A.; Barney, M.; von Hippel, P. H.; Marcus, A. H. Sub-millisecond Conformational Transitions of Short Single-stranded DNA Lattices by Photon Correlation Single-molecule FRET. *J. Phys. Chem. B* **2021**, *125*, 9426−9440.

https://doi.org/10.1021/acs.jpclett.1c03848
J. Phys. Chem. Lett. 2022, 13, 1863−1871